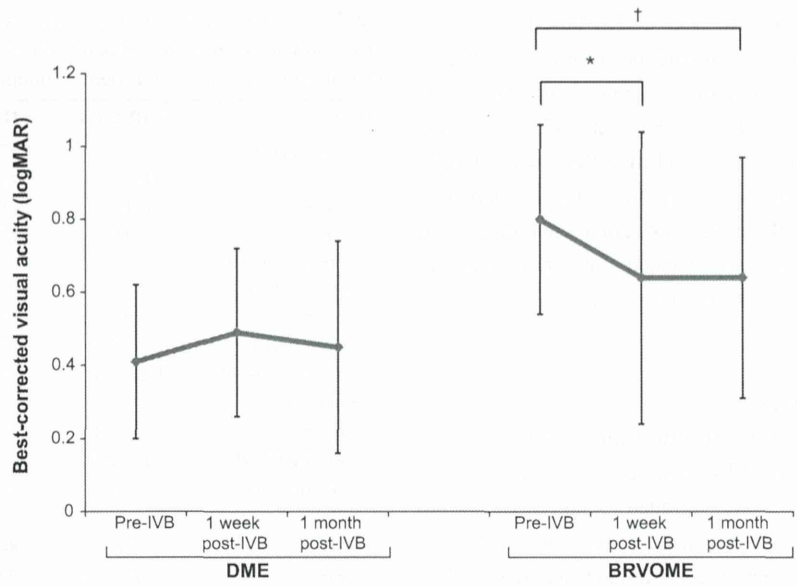


**Figure 1** Best-corrected visual acuity before and after intravitreal injection of bevacizumab.
**Notes:** BCVA did not change significantly after 1 week or 1 month in the DME group ($P$=0.34) but did in the BRVOME group ($P$=0.049), with the most significant improvement being 1 week after IVB ($P$=0.03); Freidman test compared between three points pre-IVB, 1 week post-IVB, 1 month post-IVB; †$P$<0.05, Scheffe's paired comparison compares between groups, *$P$<0.05.
**Abbreviations:** BCVA, best-corrected visual acuity; BRVOME, branch retinal vein occlusion-associated macular edema; DME, diabetic macular edema; IVB, intravitreal bevacizumab; logMAR, logarithm of the minimum angle resolution.

There are no reports on the influence of IVB on intraocular microcirculation predating the current study. Our study, in which we analyzed the results of only a single injection, broadly agrees with existing reports showing that IVB leads to a significant improvement in FT and BCVA in patients with BRVOME.[5,9] Some earlier papers also found a similar improvement in patients with DME,[28–30] but our study contradicts such findings. The exact reason for this discrepancy is unclear, but it may be related to differences in injection times and follow-up periods, pre-IVB BCVA, differences in the demographics of the DME patients, or the small number of participants in this study. One of the most interesting findings of this study, that IVB reduces MBR in all regions of the eye in patients with DME, has not been previously reported. Previous reports on post-IVB ocular circulation used color Doppler imaging (CDI) and found that blood flow decreased after IVB in the ophthalmic artery, the posterior ciliary artery, and the central retinal artery.[12,31] These studies were unable to report on blood flow within the eye itself, however, as the intraocular vessels are too small to allow CDI to function. Access to LSFG was therefore a major advantage of this study since it allowed us to directly measure MBR in the retinal vessel, ONH, and choroid and confirm the reduction of ocular blood flow in eyes with DME. We also observed a decrease in choroidal MBR in the BRVOME group, most likely because, as shown in previous reports,[32,33] the choroid lacks an autoregulation system and is easily affected by exercise. Our findings for the choroid were based on measurements taken of the MBR in retinal regions lacking large vessels, in accord with established practice for LSFG measurement of the choroid.[34]

Another interesting finding of our study was that the lack of structural improvement in the DME patients may have been related to the decrease in MBR in the ONH observed before

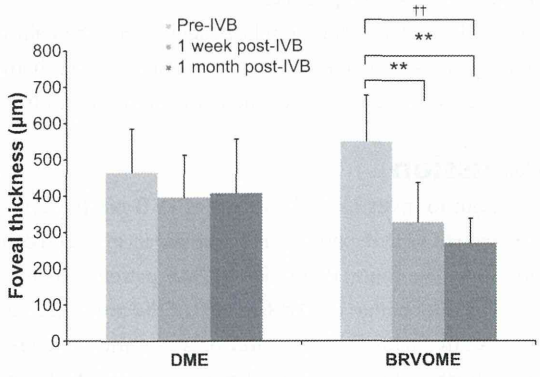


**Figure 2** Foveal thickness before and after intravitreal injection of bevacizumab.
**Notes:** FT did not change significantly 1 week or 1 month after IVB in the DME group ($P$=0.20), but did in the BRVOME group ($P$<0.001). FT improved in patients with BRVOME both 1 week and 1 month after IVB ($P$=0.007 and $P$<0.001, respectively); Friedman test compared between three points pre-IVB, 1 week post-IVB, 1 month post-IVB; ††$P$<0.01; Scheffe's paired comparison compared between groups, **$P$<0.01.
**Abbreviations:** BRVOME, branch retinal vein occlusion-associated macular edema; DME, diabetic macular edema; FT, foveal thickness; IVB, intravitreal bevacizumab.

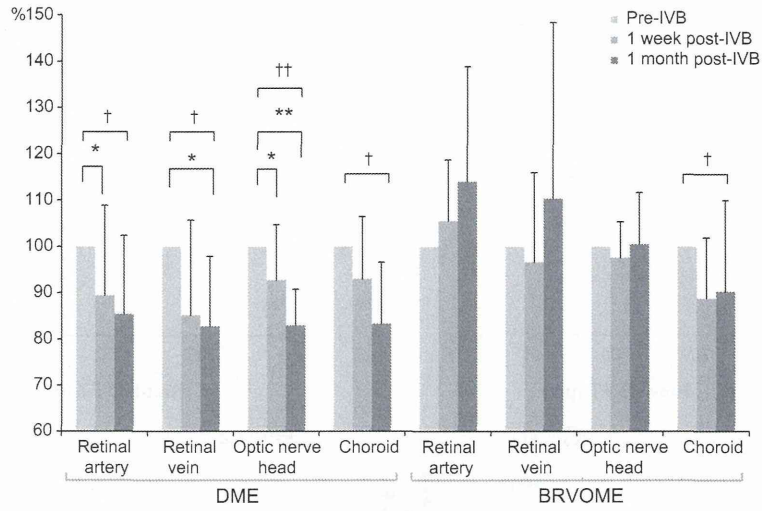


**Figure 3** Mean blur rate in the retinal artery, retinal vein, optic nerve head, and choroid before and after intravitreal injection of bevacizumab.

**Notes:** In patients with DME, a comparison of MBR values before, 1 week after, and 1 month after IVB revealed significant changes in all measured regions (retinal artery, $P$=0.02; retinal vein, $P$=0.04; ONH, $P$<0.001; and choroid, $P$=0.04). MBR after 1 week fell significantly in the retinal artery by 10.6% ($P$=0.03) and in the ONH by 7.27% ($P$=0.049). MBR after 1 week also fell by 14.8% ($P$=0.19) in the retinal vein and by 6.97% ($P$=0.15) in the choroid, but these differences were not significant. MBR after 1 month fell significantly in the retinal vein by 17.3% ($P$=0.049) and in the ONH by 17.1% ($P$<0.001). MBR after 1 month also fell by 14.7% in the retinal artery ($P$=0.08) and 16.7% in the choroid ($P$=0.06), but these differences were not significant. In patients with BRVOME, a comparison of MBR values before, 1 week after, and 1 month after IVB revealed a significant change only in the choroid ($P$=0.04). Significant changes in MBR were not observed in the retinal artery ($P$=0.09), retinal vein ($P$=0.33), or the ONH ($P$=0.50). Significant changes in blood flow were not found after 1 week in any of the measured regions (retinal artery, $P$=0.39; retinal vein, $P$=0.84; ONH, $P$=0.50; and choroid, $P$=0.09). Furthermore, significant changes were not found in blood flow after 1 month in any of the measured regions (retinal artery, $P$=0.10; retinal vein, $P$=0.67; ONH, $P$=0.84; and choroid, $P$=0.07). Finally, significant changes were not found when comparing blood flow 1 week and 1 month after IVB in any of the regions (retinal artery, $P$=0.73; retinal vein, $P$=0.33; ONH, $P$=0.84; and choroid, $P$=1.00); Friedman test compared between points pre-IVB, 1 week post-IVB, 1 month post-IVB; $^{\dagger}P$<0.05, $^{\dagger\dagger}P$<0.01; Scheffe's paired comparison compares between groups, $^{*}P$<0.05, $^{**}P$<0.01.

**Abbreviations:** BRVOME, branch retinal vein occlusion-associated macular edema; DME, diabetic macular edema; IVB, intravitreal bevacizumab; MBR, mean blur rate; ONH, optic nerve head.

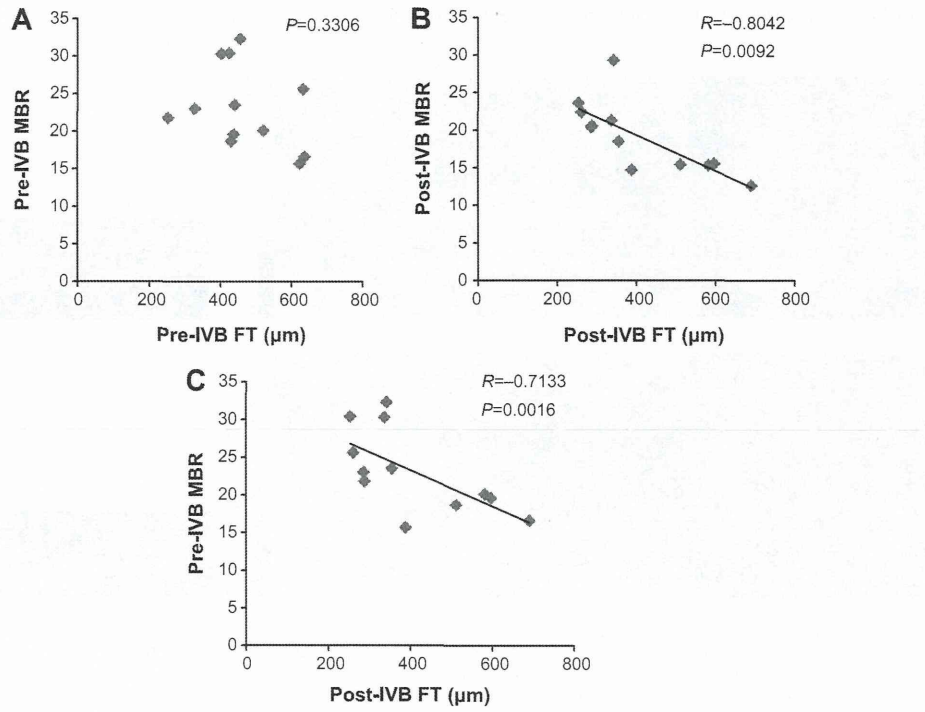


**Figure 4** Relationship between foveal thickness and mean blur rate in eyes with diabetic macular edema.

**Notes:** Pre-IVB MBR was not correlated with pre-IVB FT ($P$=0.33) (**A**). However, post-IVB MBR was correlated with post-IVB FT ($R$= –0.80, $P$=0.01) (**B**). Furthermore, pre-IVB MBR was correlated with post-IVB FT ($R$= –0.71, $P$=0.002) (**C**). One MBR sample is represented by one pixel.

**Abbreviations:** FT, foveal thickness; IVB, intravitreal bevacizumab; MBR, mean blur rate.

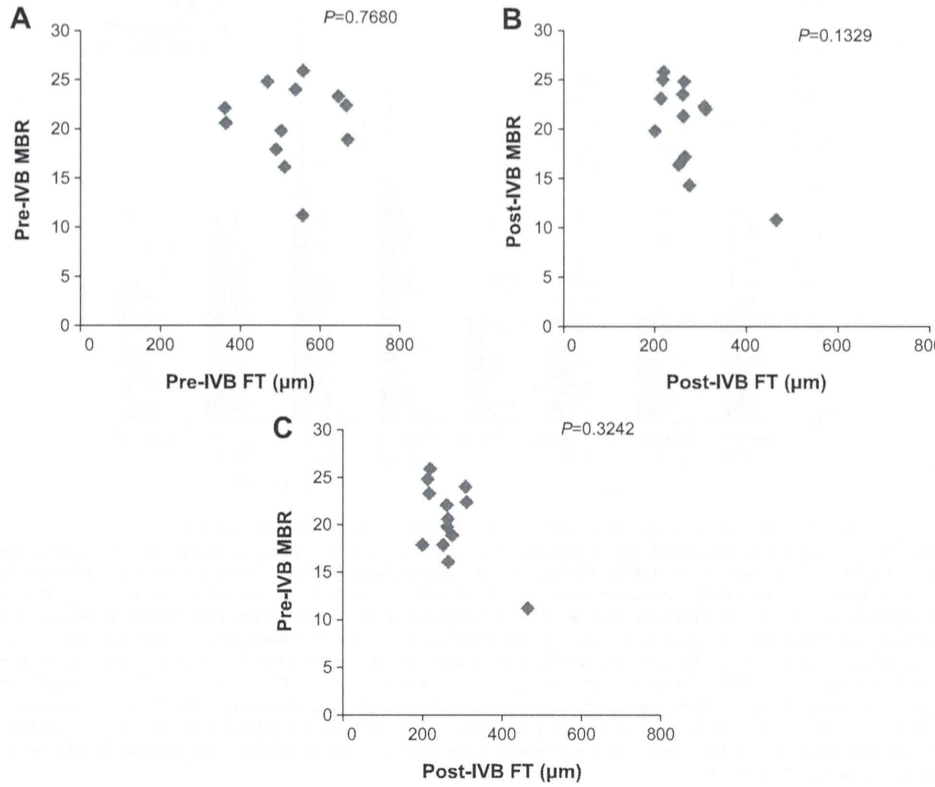


**Figure 5** Relationship between foveal thickness and mean blur rate in eyes with branch retinal vein occlusion-associated macular edema.
**Notes:** Pre-IVB MBR was not correlated with pre-IVB FT ($P$=0.77) (**A**), nor was post-IVB MBR correlated with post-IVB FT ($P$=0.13) (**B**). In addition, pre-IVB MBR was not correlated with post-IVB FT ($P$=0.32) (**C**). One MBR sample is represented by one pixel.
**Abbreviations:** FT, foveal thickness; IVB, intravitreal bevacizumab; MBR, mean blur rate.

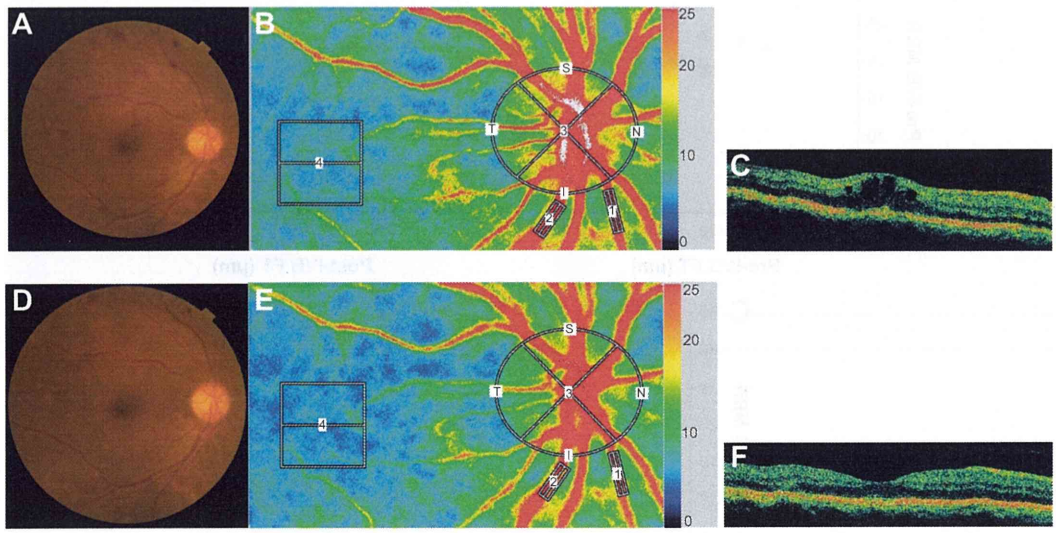


**Figure 6** Representative eye with diabetic macular edema.
**Notes:** Images from a 59-year-old man with DME in his right eye; Fundus color photographs (**A** and **D**), color LSFG maps (**B** and **E**), and axial OCT images at fovea (**C** and **F**) are shown. Pre-IVB findings are above (**A**, **B**, and **C**) and findings 1 month after IVB are below (**D**, **E**, and **F**). In the color LSFG maps (**B** and **E**), the numbers 1 and 2 indicate the rectangular scanning areas for the retinal artery and vein, respectively; 3 and 4 indicate the circular and square scanning areas for the optic nerve head and choroid, respectively. Pre-IVB MBR was 30.1 in the retinal artery, 43.6 in the retinal vein, 31.0 in the optic nerve head, and 7.0 in the choroid. MBR 1 month after IVB was 22.6 (24.9% decrease) in the retinal artery, 30.3 (30.5% decrease) in the retinal vein, 24.2 (21.9% decrease) in the optic nerve head, and 5.8 (17.1% decrease) in the choroid. Decimal best-corrected visual acuity in the right eye was 0.3 before IVB and did not change 1 month after IVB. FT in the right eye was 425 μm before IVB and 272 μm 1 month after IVB.
**Abbreviations:** DME, diabetic macular edema; FT, foveal thickness; IVB, intravitreal bevacizumab; LSFG, laser speckle flowgraphy; MBR, mean blur rate; OCT, optical coherence tomography.

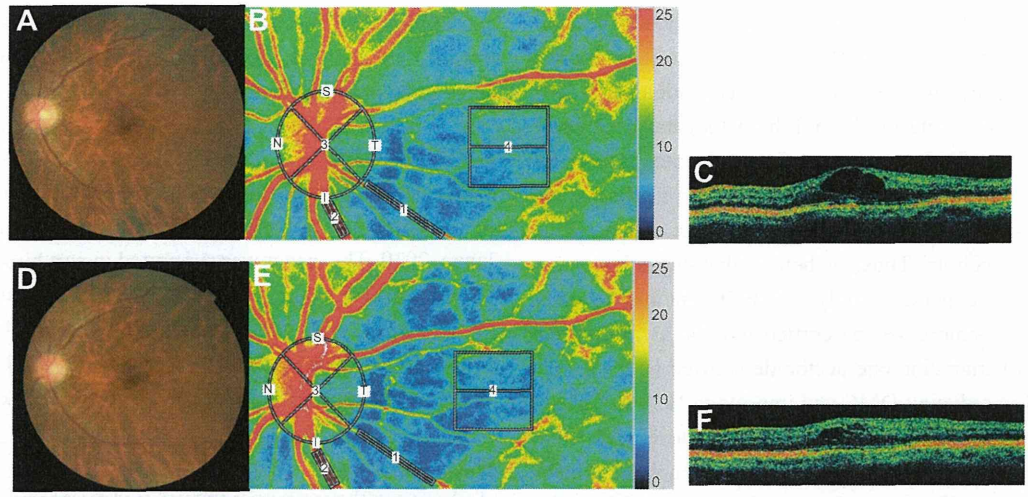


**Figure 7** Representative eye with branch retinal vein occlusion-associated macular edema.
**Notes:** Images from a 65-year-old woman with BRVOME in her left eye. Fundus color photographs (**A** and **D**), color LSFG maps (**B** and **E**), and axial OCT images at fovea (**C** and **F**) are shown. Pre-IVB findings are above (**A**, **B**, and **C**) and findings 1 month after IVB are below (**D**, **E**, and **F**). In the color LSFG maps (**B** and **E**), the numbers 1 and 2 indicate the rectangular scanning areas for the retinal artery and vein, respectively; 3 and 4 indicate the circular and square scanning areas for the optic nerve head and choroid, respectively. Pre-IVB MBR was 15.9 in the retinal artery, 35.7 in the retinal vein, 23.5 in the optic nerve head, and 7.2 in the choroid. MBR 1 month after IVB was 14.0 (12.0% decrease) in the retinal artery, 33.4 (6.4% decrease) in the retinal vein, 26.0 (10.6% increase) in the optic nerve head, and 6.2 (13.9% decrease) in the choroid. Decimal best-corrected visual acuity in the right eye was 0.5 before IVB and did not change after 1 month. FT in the right eye was 364 μm before IVB and 264 μm 1 month after IVB.
**Abbreviations:** BRVOME, branch retinal vein occlusion-associated macular edema; FT, foveal thickness; IVB, intravitreal bevacizumab; LSFG, laser speckle flowgraphy; MBR, mean blur rate; OCT, optical coherence tomography.

IVB and 1 month after IVB. We observed no such association in the BRVO group. This is an interesting discrepancy that may be related to the pathogenesis of each type of macular edema. However, it should be noted that the characteristics of the two groups in our study did not match perfectly, differing in sex distribution and pre-IVB BCVA. From these results, however, we believe that it is fair to speculate that the effect of bevacizumab on intraocular tissues changes in the presence of systemic diseases such as diabetes. In our study, the eyes with DME probably experienced the effects of excessive VEGF over the entire retina, while the effects were limited to the obstructed retinal vein and its surrounding tissues in the eyes with BRVOME. The eyes with BRVOME even showed an increase in MBR after IVB, particularly in the artery, although we could not confirm the significance of the difference statistically. If such an increase occurs, it is likely to be part of retinal autoregulation, as a compensatory increase in arterial flow rate to maintain retinal circulation. We believe that this is because in eyes with BRVOME, the retinal vessels are less damaged than in eyes with DME. Most studies of DR have noted upregulation of inducible nitric oxide synthase,[35,36] with subsequent capillary degeneration, pericyte loss and permeability.[37,38] Though the status of ocular blood flow in DR is still the subject of debate,[39,40] CDI and laser Doppler flowmetry have revealed that the velocity of blood flow in the ophthalmic artery and choroidal blood flow both decrease in eyes with DR.[41,42] We believe that retinal autoregulation may be impaired in patients with DR and, furthermore, that the additional decrease in retinal circulation caused by IVB leads to an acceleration of the original chronic ischemia in eyes with DR, explaining the appearance of macular ischemia after IVB in patients with underlying diseases such as diabetes.[14,15] Caution is therefore indicated when administering anti-VEGF antibodies, including bevacizumab, to DR patients. Even in eyes with BRVOME, although IVB can lead to a temporary reduction of the condition, we cannot exclude the possibility that IVB may also cause an adverse reduction in ocular circulation, particularly in the choroid. Thus, follow-up care in patients undergoing IVB should include LSFG examinations of ocular blood circulation, in addition to standard examinations of retinal structure and function.

It is difficult to make a prognosis on the structure and function of eyes with macular edema after IVB, especially for eyes with DME. Several biochemical mechanisms may contribute to the vascular disruptions that characterize DR and DME.[43] The pathogenesis of DME is still unclear but is thought to have several clinical aspects, including inflammation, disruption of the capillary barrier, and dysfunction of the retinal pigment epithelium. In our study, pre-IVB MBR in the ONH was significantly correlated with post-IVB FT of eyes with DME, a result indicating that IVB is not effective for patients with DME and low MBR. We believe that MBR of the ONH can be regarded as a clinically reliable preintervential parameter, and that the predictive value of pre-IVB

MBR may prove to be of importance, especially because LSFG measurements of MBR in the ONH have been reported to be highly reproducible.[44] In fact, IVB is not always fully effective in reducing DME, and the pathogenesis of DME may include an IVB-sensitive mechanism related to vascular hyperpermeability (elevated MBR) and a non-IVB-sensitive mechanism, possibly related to impairment of the retinal pigment epithelium. Thus, we believe that the pathogenesis of DME may depend not only on VEGF, but also on other mechanisms suppressed by corticosteroids, as intravitreal injection of triamcinolone acetonide showed better results than IVB in reducing DME and improving BCVA.[45] There are also reports showing that BRVOME is closely related to intraocular levels of cytokines such as macrophage inflammatory protein-1β and interleukin-6 but not of VEGF.[46,47]

Our study was limited by a small sample size, the exclusion of types of macular edema besides BRVOME and DME, the restriction of the data to 1 month after IVB, and by the fact that characteristics were not matched between the two groups. We were also not able to find more than a weak connection between visual acuity and MBR. Nevertheless, we believe our results show that in eyes with BRVOME, IVB is currently a good choice to aid in recovery of FT and visual acuity, without a concomitant decrease in retinal blood flow, at least until such time as other antibodies are ready for clinical use. Furthermore, we are the first to report that pre-IVB MBR is significantly correlated with post-IVB FT in patients with DME, indicating the possible existence of VEGF- and MBR-dependent DME.

In conclusion, we found that in patients with BRVOME, there was no significant change in MBR in the retinal artery, retinal vein, or ONH. In patients with DME, MBR in all measured areas decreased significantly. Furthermore, pre-IVB MBR was significantly correlated with post-IVB FT in patients with DME, but there was no such correlation in patients with BRVOME. Higher pre-IVB MBR in these patients was an indicator of lower post-IVB FT. Measuring MBR with LSFG, therefore, has the potential to serve as a noninvasive and objective biomarker to help clinicians determine the value of IVB treatments for patients with DME. The focus of further investigation should be a determination of MBR relationship to the mechanism behind IVB-induced reduction of DME and BRVOME.

## Author contributions

HK and TN were responsible for the design and conduct of the study. FN, HK, NA, KO, YS, and MY were responsible for the collection, management, analysis, and interpretation of the data. HK and TN were responsible for the preparation, review, and approval of the manuscript. All authors contributed toward data analysis, drafting and revising the paper and agree to be accountable for all aspects of the work.

## Disclosure

This paper was partially presented at the 27th Annual Meeting of the Japanese Society for Ocular Circulation, Kobe, Japan, 2010. This paper was supported in part by JST grant, JSPS KAKENHI Grant-in-Aid for Scientific Research (B) (T.N. 26293372), for Scientific Research (C) (H.K. 26462629), and for Exploratory Research (T.N. 26670751). The authors report no conflicts of interest in this work.

## References

1. Argon laser photocoagulation for macular edema in branch vein occlusion. The Branch Vein Occlusion Study Group. *Am J Ophthalmol.* 1984; 98(3):271–282.
2. Ferris FL 3rd, Patz A. Macular edema: a major complication of diabetic retinopathy. *Trans New Orleans Acad Ophthalmol.* 1983;31: 307–316.
3. Gutman FA, Zegarra H. Macular edema secondary to occlusion of the retinal veins. *Surv Ophthalmol.* 1984;28 Suppl:462–470.
4. Sigelman J. Diabetic macular edema in juvenile- and adult-onset diabetes. *Am J Ophthalmol.* 1980;90(3):287–296.
5. Yilmaz T, Cordero-Coma M. Use of bevacizumab for macular edema secondary to branch retinal vein occlusion: a systematic review. *Graefes Arch Clin Exp Ophthalmol.* 2012;250(6):787–793.
6. Kang HM, Chung EJ, Kim YM, Koh HJ. Spectral-domain optical coherence tomography (SD-OCT) patterns and response to intravitreal bevacizumab therapy in macular edema associated with branch retinal vein occlusion. *Graefes Arch Clin Exp Ophthalmol.* 2013;251(2): 501–508.
7. Shimura M, Yasuda K, Yasuda M, Nakazawa T. Visual outcome after intravitreal bevacizumab depends on the optical coherence tomographic patterns of patients with diffuse diabetic macular edema. *Retina.* 2013; 33(4):740–747.
8. Solaiman KA, Diab MM, Dabour SA. Repeated intravitreal bevacizumab injection with and without macular grid photocoagulation for treatment of diffuse diabetic macular edema. *Retina.* 2013;33(8):1623–1629.
9. Siegel RA, Dreznik A, Mimouni K, Bor E, Weinberger D, Bourla DH. Intravitreal bevacizumab treatment for macular edema due to branch retinal vein occlusion in a clinical setting. *Curr Eye Res.* 2012;37(9): 823–829.
10. Hanada N, Iijima H, Sakurada Y, Imasawa M. Recurrence of macular edema associated with branch retinal vein occlusion after intravitreal bevacizumab. *Jpn J Ophthalmol.* 2012;56(2):165–174.
11. Gulkilik G, Taskapili M, Kocabora S, Muftuoglu G, Demirci G. Intravitreal bevacizumab for persistent macular edema with proliferative diabetic retinopathy. *Int Ophthalmol.* 2010;30(6):697–702.
12. Hosseini H, Lotfi M, Esfahani MH, et al. Effect of intravitreal bevacizumab on retrobulbar blood flow in injected and uninjected fellow eyes of patients with neovascular age-related macular degeneration. *Retina.* 2012;32(5):967–971.
13. Matsuyama K, Ogata N, Matsuoka M, Wada M, Takahashi K, Nishimura T. Plasma levels of vascular endothelial growth factor and pigment epithelium-derived factor before and after intravitreal injection of bevacizumab. *Br J Ophthalmol.* 2010;94(9):1215–1218.
14. Shimura M, Yasuda K. Macular ischaemia after intravitreal bevacizumab injection in patients with central retinal vein occlusion and a history of diabetes and vascular disease. *Br J Ophthalmol.* 2010;94(3): 381–383.
15. Huang ZL, Lin KH, Lee YC, Sheu MM, Tsai RK. Acute vision loss after intravitreal injection of bevacizumab (avastin) associated with ocular ischemic syndrome. *Ophthalmologica.* 2010;224(2):86–89.

16. Yoshida Y, Sugiyama T, Utsunomiya K, Ogura Y, Ikeda T. A pilot study for the effects of donepezil therapy on cerebral and optic nerve head blood flow, visual field defect in normal-tension glaucoma. *J Ocul Pharmacol Ther*. 2010;26(2):187–192.
17. Sugiyama T, Kojima S, Ishida O, Ikeda T. Changes in optic nerve head blood flow induced by the combined therapy of latanoprost and beta blockers. *Acta Ophthalmol*. 2009;87(7):797–800.
18. Takahashi H, Sugiyama T, Tokushige H, et al. Comparison of CCD-equipped laser speckle flowgraphy with hydrogen gas clearance method in the measurement of optic nerve head microcirculation in rabbits. *Exp Eye Res*. 2013;108:10–15.
19. Wang L, Cull GA, Piper C, Burgoyne CF, Fortune B. Anterior and posterior optic nerve head blood flow in nonhuman primate experimental glaucoma model measured by laser speckle imaging technique and microsphere method. *Invest Ophthalmol Vis Sci*. 2012;53(13):8303–8309.
20. Nagahara M, Tamaki Y, Araie M, Fujii H. Real-time blood velocity measurements in human retinal vein using the laser speckle phenomenon. *Jpn J Ophthalmol*. 1999;43(3):186–195.
21. Nagahara M, Tamaki Y, Tomidokoro A, Araie M. In vivo measurement of blood velocity in human major retinal vessels using the laser speckle method. *Invest Ophthalmol Vis Sci*. 2011;52(1):87–92.
22. Aizawa N, Kunikata H, Yokoyama Y, Nakazawa T. Correlation between optic disc microcirculation in glaucoma measured with laser speckle flowgraphy and fluorescein angiography, and the correlation with mean deviation. *Clin Experiment Ophthalmol*. 2014;42(3):293–294.
23. Yokoyama Y, Aizawa N, Chiba N, et al. Significant correlations between optic nerve head microcirculation and visual field defects and nerve fiber layer loss in glaucoma patients with myopic glaucomatous disk. *Clin Ophthalmol*. 2011;5:1721–1727.
24. Chiba N, Omodaka K, Yokoyama Y, et al. Association between optic nerve blood flow and objective examinations in glaucoma patients with generalized enlargement disc type. *Clin Ophthalmol*. 2011;5:1549–1556.
25. Sugiyama T, Araie M, Riva CE, Schmetterer L, Orgul S. Use of laser speckle flowgraphy in ocular blood flow research. *Acta Ophthalmol*. 2010;88(7):723–729.
26. Fabick MM. Ethical considerations for research on human subjects. *Plast Surg Nurs*. 1995;15(4):225–227, 231.
27. Enserink M. Bioethics. Helsinki's new clinical rules: fewer placebos, more disclosure. *Science*. 2000;290(5491):418–419.
28. Forte R, Cennamo GL, Finelli M, et al. Intravitreal bevacizumab vs intravitreal triamcinolone combined with macular laser grid for diffuse diabetic macular oedema. *Eye (Lond)*. 2010;24(8):1325–1330.
29. Arevalo JF, Sanchez JG, Wu L, et al; Pan-American Collaborative Retina Study Group. Primary intravitreal bevacizumab for diffuse diabetic macular edema: the Pan-American Collaborative Retina Study Group at 24 months. *Ophthalmology*. 2009;116(8):1488–1497, 1497.e1.
30. Paccola L, Costa RA, Folgosa MS, Barbosa JC, Scott IU, Jorge R. Intravitreal triamcinolone versus bevacizumab for treatment of refractory diabetic macular oedema (IBEME study). *Br J Ophthalmol*. 2008;92(1):76–80.
31. Bonnin P, Pournaras JA, Lazrak Z, et al. Ultrasound assessment of short-term ocular vascular effects of intravitreal injection of bevacizumab (Avastin®) in neovascular age-related macular degeneration. *Acta Ophthalmol*. 2010;88(6):641–645.
32. Okuno T, Sugiyama T, Kohyama M, Kojima S, Oku H, Ikeda T. Ocular blood flow changes after dynamic exercise in humans. *Eye (Lond)*. 2006;20(7):796–800.
33. Shiga Y, Shimura M, Asano T, Tsuda S, Yokoyama Y, Aizawa N, Omodaka K, et al. The influence of posture change on ocular blood flow in normal subjects, measured by laser speckle flowgraphy. *Curr Eye Res*. 2013;38(6):691–698.
34. Isono H, Kishi S, Kimura Y, Hagiwara N, Konishi N, Fujii H. Observation of choroidal circulation using index of erythrocytic velocity. *Arch Ophthalmol*. 2003;121(2):225–231.
35. Carmo A, Cunha-Vaz JG, Carvalho AP, Lopes MC. Nitric oxide synthase activity in retinas from non-insulin-dependent diabetic Goto-Kakizaki rats: correlation with blood-retinal barrier permeability. *Nitric Oxide*. 2000;4(6):590–596.
36. Abu El-Asrar AM, Desmet S, Meersschaert A, Dralands L, Missotten L, Geboes K. Expression of the inducible isoform of nitric oxide synthase in the retinas of human subjects with diabetes mellitus. *Am J Ophthalmol*. 2001;132(4):551–556.
37. Zheng L, Du Y, Miller C, et al. Critical role of inducible nitric oxide synthase in degeneration of retinal capillaries in mice with streptozotocin-induced diabetes. *Diabetologia*. 2007;50(9):1987–1996.
38. Leal EC, Manivannan A, Hosoya K, et al. Inducible nitric oxide synthase isoform is a key mediator of leukostasis and blood-retinal barrier breakdown in diabetic retinopathy. *Invest Ophthalmol Vis Sci*. 2007;48(11):5257–5265.
39. Grunwald JE, Brucker AJ, Grunwald SE, Riva CE. Retinal hemodynamics in proliferative diabetic retinopathy. A laser Doppler velocimetry study. *Invest Ophthalmol Vis Sci*. 1993;34(1):66–71.
40. Patel V, Rassam S, Newsom R, Wiek J, Kohner E. Retinal blood flow in diabetic retinopathy. *BMJ*. 1992;305(6855):678–683.
41. Gracner T. Ocular blood flow velocity determined by color Doppler imaging in diabetic retinopathy. *Ophthalmologica*. 2004;218(4):237–242.
42. Nagaoka T, Kitaya N, Sugawara R, et al. Alteration of choroidal circulation in the foveal region in patients with type 2 diabetes. *Br J Ophthalmol*. 2004;88(8):1060–1063.
43. Ciulla TA, Amador AG, Zinman B. Diabetic retinopathy and diabetic macular edema: pathophysiology, screening, and novel therapies. *Diabetes Care*. 2003;26(9):2653–2664.
44. Aizawa N, Yokoyama Y, Chiba N, et al. Reproducibility of retinal circulation measurements obtained using laser speckle flowgraphy-NAVI in patients with glaucoma. *Clin Ophthalmol*. 2011;5:1171–1176.
45. Shimura M, Nakazawa T, Yasuda K, et al. Comparative therapy evaluation of intravitreal bevacizumab and triamcinolone acetonide on persistent diffuse diabetic macular edema. *Am J Ophthalmol*. 2008;145(5):854–861.
46. Shimura M, Nakazawa T, Yasuda K, Kunikata H, Shiono T, Nishida K. Visual prognosis and vitreous cytokine levels after arteriovenous sheathotomy in branch retinal vein occlusion associated with macular oedema. *Acta Ophthalmol*. 2008;86(4):377–384.
47. Kunikata H, Shimura M, Nakazawa T, et al. Chemokines in aqueous humour before and after intravitreal triamcinolone acetonide in eyes with macular oedema associated with branch retinal vein occlusion. *Acta Ophthalmol*. 2012;90(2):162–167.

Journal of Neuroscience Research

Journal of Neuroscience Research 92:1134–1142 (2014)

# Critical Neuroprotective Roles of Heme Oxygenase-1 Induction Against Axonal Injury-Induced Retinal Ganglion Cell Death

**Noriko Himori, Kazuichi Maruyama, Kotaro Yamamoto, Masayuki Yasuda, Morin Ryu, Kazuko Omodaka, Yukihiro Shiga, Yuji Tanaka, and Toru Nakazawa***

Department of Ophthalmology, Tohoku University Graduate School of Medicine, Miyagi, Japan

Although axonal damage induces significant retinal ganglion cell (RGC) death, small numbers of RGCs are able to survive up to 7 days after optic nerve crush (NC) injury. To develop new treatments, we set out to identify patterns of change in the gene expression of axonal damage-resistant RGCs. To compensate for the low density of RGCs in the retina, we performed retrograde labeling of these cells with 4Di-10ASP in adult mice and 7 days after NC purified the RGCs with fluorescence-activated cell sorting. Gene expression in the cells was determined with a microarray, and the expression of *Ho-1* was determined with quantitative PCR (qPCR). Changes in protein expression were assessed with immunohistochemistry and immunoblotting. Additionally, the density of Fluoro-gold-labeled RGCs was counted in retinas from mice pretreated with CoPP, a potent HO-1 inducer. The microarray and qPCR analyses showed increased expression of *Ho-1* in the post-NC RGCs. Immunohistochemistry also showed that HO-1-positive cells were present in the ganglion cell layer (GCL), and cell counting showed that the proportion of HO-1-positive cells in the GCL rose significantly after NC. Seven days after NC, the number of RGCs in the CoPP-treated mice was significantly higher than in the control mice. Combined pretreatment with SnPP, an HO-1 inhibitor, suppressed the neuroprotective effect of CoPP. These results reflect changes in HO-1 activity to RGCs that are a key part of RGC survival. Upregulation of HO-1 signaling may therefore be a novel therapeutic strategy for glaucoma. 

**Key words:** heme oxygenase-1; retinal ganglion cell; glaucoma; neuroprotection

According to global surveys (Quigley, 1996), glaucoma is the second most common cause of blindness, after cataracts. It is the foremost type of optic neuropathy, in which the ultimate cause of vision loss is thought to be retinal ganglion cell (RGC) apoptosis (Yücel et al., 2003). The RGCs are the only neurons connected to the brain by the optic nerve, and a significant dying off of these cells is characteristic of glaucoma. There are a variety of mechanisms causing RGC death, including oxidative stress (Izzotti et al., 2006; Ferreira et al., 2010; Yuki et al., 2011), excitatory amino acids such as glutamate (Sullivan et al., 2006; Harada et al., 2007), endoplasmic reticulum stress (Uchibayashi et al., 2011), and nitric oxide (Neufeld et al., 1999). Therefore, neuroprotection of the RGCs has recently drawn attention as a new approach to glaucoma therapy.

Several studies have provided evidence that oxidative stress and the related damage contribute to glaucomatous degeneration of the RGCs (Tezel, 2006). Oxidative-stress-induced change can either cause RGC damage and death directly or trigger downstream effects (Tezel, 2006). Although an elevated intraocular pressure (higher than 21 mmHg) is the greatest risk factor for primary open-angle glaucoma, normal-tension glaucoma (NTG), the most common type worldwide and the prevalent type in Asia (Iwase et al. 2004), occurs in eyes with normal intraocular pressure (10–21 mmHg). The pathogenesis of RGC death in NTG has yet to be elucidated, even though the vulnerability of the RGCs is well known. Nerve crush (NC) is a commonly used model of axonal injury that provides insight into the mechanisms involved in the death of the RGCs. It involves applying a precise, short-term,

Contract grant sponsor: Ministry of Education, Science and Technology of Japan; Contract grant number: 23592613 (to K.M). This paper was supported in part by JSPS KAKENHI Grant-in-Aid for Scientific Research (B) (T.N. 26293372), for Exploratory Research (T.N. 26670751), and for young scientists (N.H. 26861434).

*Correspondence to: Toru Nakazawa, MD, PhD, Tohoku University Graduate School of Medicine, Department of Ophthalmology, 1-1 Seiryo, Aoba, Sendai, Miyagi 980-8574, Japan.
E-mail: ntoru@fa2.so-net.ne.jp

Received 17 February 2014; Revised 10 March 2014; Accepted 1 April 2014

**Published online 5 May 2014 in Wiley Online Library (wileyonlinelibrary.com). DOI: 10.1002/jnr.23398**

synchronous insult to the axons, which results in secondary RGC apoptotic cell death resembling glaucoma.

Several studies have used microarrays for genome-wide analysis of the retina in models of glaucoma and in DBA/2J mice (Steele et al., 2006; Panagis et al., 2010). The RGCs represent only a small percentage of the total cell population in the retina, however, and microarray analysis can miss many responses specific to the RGCs. To supplement the broad analysis provided by microarray, therefore, we also used fluorescence-activated cell sorting (FACS) to isolate the RGCs from other cells in the retina.

Heme oxygenase (HO), the rate-limiting enzyme in heme catabolism, catalyzes the degradation of heme to biliverdin, with the concurrent release of iron and carbon monoxide. Three isoforms have been identified, HO-1, HO-2, and HO-3 (Mancuso, 2004). HO-1 (also known as *heat-shock protein 32*) is induced by certain cellular stress conditions, including heat shock (Shibahara et al., 1987), oxidative damage (Keyse and Tyrrell, 1989), and ischemia–reperfusion injury (Takeda et al., 1994). The use of gene transfer or drugs to induce HO-1 has been shown to inhibit apoptosis and to provide cellular protection after injury (Li Volti et al., 2007; Lai et al., 2008; Peng et al., 2008, 2011). Recently, such newly proposed neuroprotective strategies have become the subject of investigation as new goals for glaucoma therapy (Lebrun-Julien and Di Polo, 2008; Weber et al., 2008). Changes during the early stages of glaucoma may increase the vulnerability of the RGCs, which might explain the progression of vision loss in patients despite IOP-lowering therapy in open angle glaucoma or in non-IOP-dependent types of glaucoma such as NTG. Insights into the mechanisms of axonal-damage-induced RGC death are therefore urgently needed to aid in the development of new neuroprotective treatment strategies for patients with glaucoma.

## MATERIALS AND METHODS

### Animals

Adult, 10-12-week-old male C57BL/B6 mice (SLC, Shizuoka, Japan), housed in covered cages, were maintained and handled in accordance with the guidelines of the ARVO Statement for the Use of Animals in Ophthalmic and Vision Research and the guidelines from the declaration of Helsinki and the Guiding Principles in the Care and Use of Animals. All experimental procedures described in the present study were approved by the Ethics Committee for Animal Experiments at Tohoku University Graduate School of Medicine, and were performed according to the National Institutes of Health *Guidelines for the care and use of laboratory animals.*

### Surgery

Retrograde labeling was performed according to established procedures (Ryu et al., 2012; Shanab et al., 2012). Briefly, the mice were anesthetized with a ketamine/xylazine mixture. The RGCs were retrogradely labeled with a fluorescent tracer, Fluoro-Gold (FG; Fluorochrome, Englewood, CO), or carbocyanine dye N-4-[4-didecylaminostryryl]-N-methyl-pyridinium iodide (4Di-10ASP; Molecular Probes, Eugene, OR). Either 3% 4Di-10ASP in dimethylformamide or 1 μl of 2% aqueous FG in 1% dimethylsulfoxide (DMSO) was injected into the superior colliculus with a 32-G needle. Seven days after FG labeling, an NC procedure was performed in the animals' right eyes.

Seven days after NC, the mice were sacrificed, and their complete retinas were placed on glass slides with the ganglion cell layer facing upward. RGC density was determined by counting tracer-labeled RGCs in 12 distinct areas under a microscope as previously described (Himori et al., 2013).

### RGC Purification and Quantitative RT-PCR (qPCR)

The 4Di-10ASP-labeled RGCs were purified according to established procedures (Himori et al., 2013). Briefly, the 4Di-10ASP-labeled mice were euthanized 7 days after NC. The retinas were rapidly dissected, incubated in a digestion solution containing papain (10 U/ml; Worthington, Lakewood, NJ) and L-cysteine (0.3 mg/ml; Sigma, St. Louis, MO) in HBSS (37°C for 15 min; $CO_2$ incubator), rinsed twice in HBSS, and then triturated to create a single-cell suspension. The dissociated cells were promptly sorted using a FACS Aria II (Becton-Dickinson, San Jose, CA). The 4Di-10ASP-labeled RGCs were detected with a 585/42 filter. The cells were sorted directly into 350 μl of buffer RLT Plus (Qiagen, Valencia, CA) with 1% β-mercaptoethanol, frozen immediately, and stored at −80°C until further use. Samples of the post-NC RGCs and non-NC controls each contained 6,000 RGCs. Total RNA was extracted from FACS-purified RGCs by using an RNeasy Micro Kit (Qiagen) according to the manufacturer's protocol. The RNA was then concentrated using RNeasy MinElute Spin columns (Qiagen), and first-strand cDNA synthesis was performed with the SuperScript III First Strand Synthesis SuperMix for qRT-PCR (Invitrogen, Carlsbad, CA). Taqman Fast Universal PCR master mix (4352042; Applied Biosystems, Foster City, CA) was used for qPCR to quantify mRNA levels by using commercially available Taqman probes for *Ho-1* (Mm00516007_m1) and *Gapdh* (Mm99999915_g1). Relative gene expression levels were calculated by using the ΔΔCt method. The mRNA levels were normalized to *Gapdh* as an internal control.

### DNA Microarray Analysis

Isolation of RGCs was performed as described above. Each sample contained ~100,000 RGCs, pooled from four to six individually sorted retinas, and yielded 50 ng of total RNA, which is enough for microarray analysis (Kurabo Industries, Osaka, Japan). We analyzed mRNA expression using GenopalR ROSM-JX chips (Mitsubishi Rayon, Tokyo, Japan) equipped with 219 oligonucleotide DNA probes in hollow plastic fibers specially designed to detect mouse mRNA sequences. Hybridization signals were analyzed using a DNA chip analyzer according to the manufacturer's instructions. DNA chip data were compared for analysis by Kurabo custom analysis services (Kurabo). Increases more than twofold were regarded as significant. The gene list is given in Table 1.

### Immunohistochemistry

Immunohistochemistry was performed according to our previous publications (Nakazawa et al., 2006, 2007). The eyes

**TABLE 1. Genes**

| Accession No. | Gene symbol | Gene description | NC− | NC+ | Ratio |
|---|---|---|---|---|---|
| NM_015760.3 | Nox4 | NADPH oxidase 4 (Nox4) | 12 | 98 | 8.30 |
| NM_009663.1 | Alox5ap | Arachidonate 5-lipoxygenase activating protein (Alox5ap) | 43 | 332 | 7.68 |
| NM_009155.3 | Sepp1 | Selenoprotein P, plasma, 1 (Sepp1) | 212 | 1,399 | 6.60 |
| NM_008871.1 | Serpine1 | Serine (or cysteine) peptidase inhibitor, clade E, member 1 (Serpine1) | 101 | 653 | 6.49 |
| NM_001037859.2 | Csf1r | Colony- stimulating factor 1 receptor (Csf1r) | 1105 | 7,041 | 6.37 |
| NM_010907.1 | Nfkbia | Nuclear factor of kappa light polypeptide gene enhancer in B-cells inhibitor, alpha (Nfkbia) | 339 | 1,974 | 5.82 |
| NM_009463.2 | Ucp1 | Uncoupling protein 1 (mitochondrial, proton carrier) (Ucp1) | 12 | 62 | 5.04 |
| NM_009740.1 | Bcl10 | B-cell leukemia/lymphoma 10 (Bcl10) | 26 | 132 | 5.00 |
| NM_010554.4 | Il1a | Interleukin 1 alpha (Il1a) | 133 | 610 | 4.60 |
| NM_001009935.2 | Txnip | Thioredoxin interacting protein (Txnip) | 212 | 969 | 4.57 |
| NM_019823.3 | Cyp2d22 | Cytochrome P450, family 2, subfamily d, polypeptide 22 (Cyp2d22) | 132 | 556 | 4.22 |
| NM_008185.2 | Gstt1 | Glutathione S-transferase, theta 1 (Gstt1) | 234 | 945 | 4.04 |
| NM_010442.1 | Hmox1 | Heme oxygenase (decycling) 1 (Hmox1) | 329 | 1,074 | 3.27 |
| NM_024264.4 | Cyp27a1 | Cytochrome P450, family 27, subfamily a, polypeptide 1 (Cyp27a1) | 104 | 335 | 3.21 |
| NM_008493.3 | Lep | Leptin (Lep) | 7 | 23 | 3.14 |
| NM_008509.2 | Lpl | Lipoprotein lipase (Lpl) | 212 | 663 | 3.12 |
| NM_001044384.1 | Timp1 | Tissue inhibitor of metalloproteinase 1 (Timp1) | 27 | 76 | 2.84 |
| NM_010361.2 | Gstt2 | Glutathione S-transferase, theta 2 (Gstt2) | 47 | 132 | 2.79 |
| NM_133994.3 | Gstt3 | Glutathione S-transferase, theta 3 (Gstt3) | 64 | 169 | 2.64 |
| NM_009744.3 | Bcl6 | B-cell leukemia/lymphoma 6 (Bcl6) | 124 | 309 | 2.50 |
| NM_008116.2 | Ggt1 | Gamma-glutamyltransferase 1 (Ggt1) | 36 | 90 | 2.49 |
| NM_011671.4 | Ucp2 | Uncoupling protein 2 (mitochondrial, proton carrier) (Ucp2) | 5 | 12 | 2.31 |
| NM_029555.2 | Gstk1 | Glutathione S-transferase kappa 1 (Gstk1) | 91 | 210 | 2.30 |
| NM_013602.2 | Mt1 | Metallothionein 1 (Mt1) | 11,218 | 25,656 | 2.29 |
| NM_010358.4 | Gstm1 | Glutathione S-transferase, mu 1 (Gstm1) | 457 | 1,044 | 2.29 |
| NM_008184.3 | Gstm6 | Glutathione S-transferase, mu 6 (Gstm6) | 37 | 83 | 2.24 |
| NM_011480.3 | Srebf1 | Sterol regulatory element binding transcription factor 1 (Srebf1) | 518 | 1,141 | 2.20 |

were enucleated as described in the histological analysis section, fixed in 4% paraformaldehyde overnight at 4°C, immersed in a 20% sucrose solution, and embedded in an optimal cutting temperature compound (Sakura Finetechnical, Tokyo, Japan). Ten-micrometer-thick cryosections were mounted on the slides and incubated with blocking buffer (10% goat serum, 0.5% gelatin, 3% BSA, and 0.2% Tween 20 in PBS). Next, they were incubated with rabbit polyclonal anti-HO-1 antibody (1:200; Enzo Life Sciences, Farmingdale, NY) and mouse monoclonal anti-C38 antibody (graciously donated by T. Wakabayashi; Wakabayashi et al., 2010) overnight at 4°C. The sections were incubated with Alexa 488 secondary antibody (1:200; Invitrogen) for 1 hr. Photographs of the retina were taken in areas 500 μm and 1,000 μm from the center of the optic nerve using fluorescence illumination (Axiovert-200; Carl Zeiss, Jena, Germany). Cell counts were performed as described previously (Nakazawa et al., 2008). Briefly, a blind count was performed of immunopositive cells colocalized with DAPI-stained nuclei from four sections of a single eye's ganglion cell layer (GCL). The numbers were then averaged.

## Experimental Protocol

Injections were prepared as follows: cobalt protoporphyrin IX (CoPP; Frontier Scientific, Logan, UT) was first dissolved in 0.1 N NaOH and further diluted to a final concentration of 0.02 N with PBS. Tin protoporphyrin (SnPP; Frontier Scientific) was dissolved in equal amounts of PBS and 0.1 N NaOH. The mice received intraperitoneal (IP) injections of CoPP (10 μmol/kg body weight) every 24 hr before NC for 3 days and after NC for 6 more days. IP injection of SnPP (10 μmol/kg body weight), when performed, was simultaneous with injection of CoPP. We then examined the number of RGCs 7 days after NC as described above.

## Immunoblot Analysis

Three days after the administration of CoPP, the retinas were isolated and placed into a lysis buffer (Thermo Fisher Scientific, Waltham, MA) containing a 1% protease inhibitor cocktail (Sigma) and a 1% phosphatase inhibitor cocktail (Sigma). Cell lysates were clarified by centrifugation at 15,000*g* at 4°C for 20 min. Each sample was separated with SDS-PAGE and electroblotted onto a polyvinylidene fluoride (PVDF) membrane (Millipore, Bedford, MA). After nonspecific binding had been blocked with 4% BlockAce (Yukijirushi, Sapporo, Japan), the membranes were incubated at 4°C overnight with a rabbit polyclonal antibody against HO-1 (1:1,000; Enzo) or β-actin (1:5,000; Sigma). The membranes were then incubated with a horseradish peroxidase-conjugated anti-mouse or anti-rabbit immunoglobulin secondary antibody for 1 hr. The signals were visualized with chemiluminescence (ECL blotting analysis system; Amersham, Arlington Heights, IL), measured in Image Lab statistical software (Bio-Rad, Hercules, CA), and normalized to β-actin.

## Statistical Analysis

All data are expressed as mean &plunmn; SD. The values were processed for statistical analysis (Mann-Whitney U test), followed by a two-tailed Student's *t*-test. Comparisons between

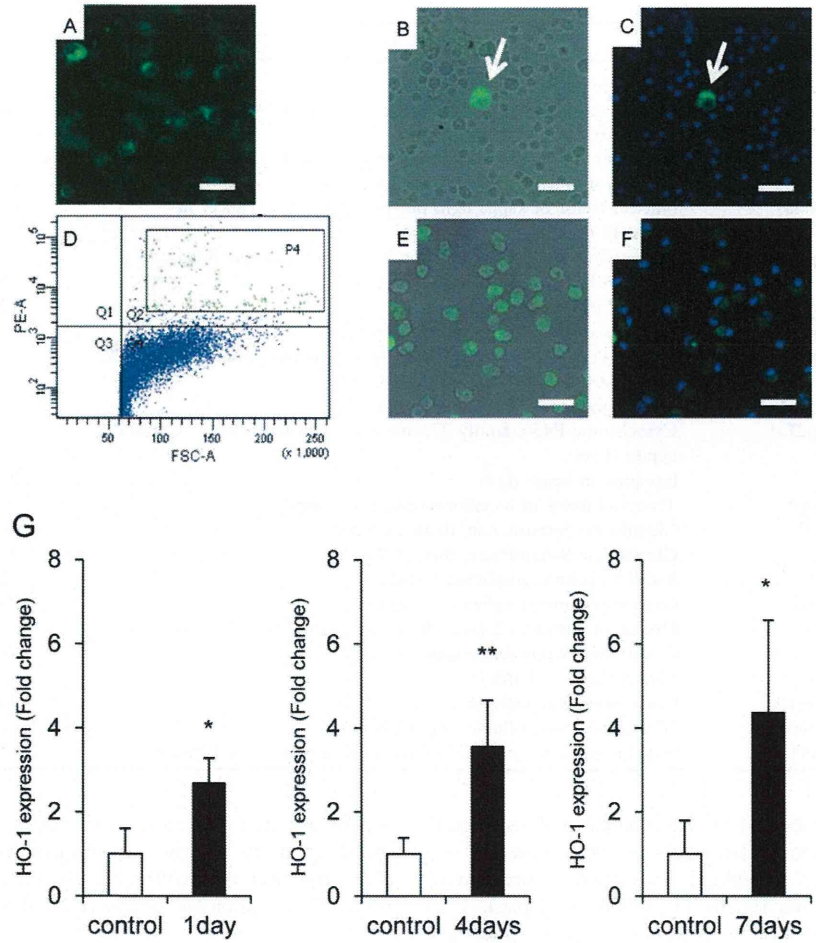


Fig. 1. RGC purification using FACS from dissociated retinas retrogradely labeled with 4Di-10ASP. **A:** Representative photograph of a flat-mount retina. The RGCs were labeled with 4Di-10ASP (green). **B,C:** Representative photographs of dissociated retinal cells before sorting. 0.2% of the cells were 4Di-10ASP+ RGCs before sorting. The arrows indicate RGCs. **D:** FACS analysis of retinal cells. **E,F:** Representative photographs of dissociated retinal cells after sorting. **G:** Graphs comparing RGC gene expression changes in control and NC mice. Changes were determined by qPCR measurements of mRNA levels in the RGCs. mRNA expression of *Ho-1* in the RGCs had increased 1 (control, n = 4; NC, n = 4), 4 (control, n = 5; NC, n = 5), and 7 (control, n = 4; NC, n = 5) days after NC. NC, nerve crush. $*P < 0.05$, $**P < 0.01$ Scale bars = 20 μm.

multiple groups were analyzed by using the Krüskal-Wallis, followed by Steel's, tests. Differences were considered statistically significant at $P < 0.05$.

## RESULTS

### Isolation of RGCs With FACS and Changes in RGC Gene Expression 7 Days After NC

RGCs were retrogradely labeled with 4Di-10ASP 7 days after NC (Fig. 1A). The ratio of 4Di-10ASP$^+$ RGCs in a sample of dissociated retinal cells before sorting was only 0.2% (Fig. 1B,C). Our FACS analysis showed that, before sorting, there were relatively few large and highly fluorescent cells in the dissociated retinas (Fig. 1D). Sorting greatly increased the proportion of these cells (Fig. 1E,F). We then examined post-NC changes in gene expression in these FACS-sorted RGCs. Table 1 shows the genes with the greatest increases in expression, as determined by microarray analysis. The expression of each of these genes increased twofold or more. We also examined the expression of the *Ho-1* gene in the purified RGCs with qPCR. Normalized to *Ho-1* expression levels in control RGCs, there were increases of 2.7 ± 0.58, 3.6 ± 1.1, and 4.4 ± 2.2 times, at 1, 4, and 7 days after NC, respectively. qPCR thus showed increased *Ho-1* expression in the RGCs at every stage following NC ($P < 0.05$, $P < 0.01$; Fig. 1G).

### Immunohistochemical Detection of HO-1 After NC

HO-1 immunoreactivity was not observed in normal retinas (Fig. 2A). However, 1, 4, and 7 days after